Author

Cheryl E. Peyser

Title

Controls on Permo-Carboniferous Precipitation over Tropical Pangea: A GCM Sensitivity Study

Submitted for Publication in:

Palaeogeography, Palaeoclimatology, Palaeoecology

in lieu of thesis in partial fulfillment
of the requirements for the degree of
Master of Science in Geology
Department of Geological Sciences
The University of Michigan

Accepted by:

Signature	Dr. Christopher J. Poulsen Name	10/01/2006 Date
Signature	Dr. David Rea Name	10/14/06 Date
Department Chair	Dr. Rodney Ewing Name	10/18/06 Date


THE UNIVERSITY OF MICHIGAN
LIBRARIES
1817

Controls on Permo-Carboniferous Precipitation over Tropical Pangea: A GCM sensitivity study

Cheryl E. Peyser
Christopher J. Poulsen
Department of Geological Sciences, University of Michigan, Ann Arbor, Michigan 48109, USA

Abstract

A series of Late Paleozoic climate model simulations was developed using the GENESIS atmospheric general circulation model to investigate the role of Gondwanan deglaciation, atmospheric CO_2 rise, and regional tectonism on continental precipitation over tropical Pangea. The model results indicate that both deglaciation and CO_2 rise from 1x to 8x present-atmospheric levels could have caused substantial drying and warming at low-latitudes, a result that is consistent with Late Paleozoic proxy records. Yet, the atmospheric processes that led to drying differ between these cases. The deglaciation of Gondwana causes the Southern Hemisphere winter cell of the Hadley circulation to decrease by as much as 60% and to shift into the Southern Hemisphere, reducing the convective precipitation over equatorial Pangea. In contrast, high levels of CO_2 have little effect on the large-scale overturning circulation but increase continental temperatures, leading to high evaporation rates and reduced available soil moisture, the source of convective precipitation on land. In comparison to deglaciation and pCO_2, regional uplift/erosion of the Central Pangean Mountains (CPMs) has a secondary effect on tropical precipitation in GENESIS and can not explain the long-term aridification and warming of western Pangea. We suggest that Late Paleozoic climate change over low-latitude Pangea likely resulted from the combined effects of deglaciation of Gondwanan ice sheets and a rise in atmospheric CO_2.

1. Introduction

Low-latitude Pangea underwent profound climate change during the Permo-Carboniferous marked by long-term drying. The occurrence of widespread peat-forming forests, high-diversity paleoflora, paleosol composition and paleosol isotopic geochemistry indicate that the paleoequator was tropical with "ever-wet", "ever-warm" conditions in the Carboniferous (Cecil, 1990; Tabor and Montañez, 2002; Raymond and Metz, 2004). Throughout the late Carboniferous and early Permian, however, these conditions gave way to seasonally-dry climates. Peat-forming forests were replaced by savannah-like flora (Cleal and Thomas, 2005); soil moisture decreased (Tabor and Montañez, 2004); and, coal beds, paleosols, and fluvial facies gave way to eolian and evaporite facies (Cecil, 1990; Rankey, 1997; Kessler et al., 2001; Tabor and Montañez, 2002; Ziegler et al., 2002). This drying trend is associated with a decrease in low-latitude floral diversity (Ziegler et al., 2002; Raymond and Metz, 2004) and a shift from spore-producing to seed-producing plants. In addition to long-term aridification, the Permo-Carboniferous paleoequator also grew ~10°C warmer (Tabor and Montañez, 2005) and, in western Pangea, winds shifted from Easterlies to Westerlies (Soreghan et al., 2002; Tabor and Montañez, 2002).

Several explanations have been given for the low-latitude Permo-Carboniferous aridity trend, emphasizing primarily tectonic controls. Importantly, equatorial Pangea did not experience appreciable latitudinal drift during this period (Scotese, 1999; Ziegler et al., 2002; Loope et al., 2004), eliminating the possibility that continental drift into the subtropics caused the drying. It has been suggested that the uplift of the Central Pangean

Mountains (CPMs), a southwest-northeast trending mountain chain consisting of the Appalachian-Mauretanide-Hercynian orogenic belts that straddled the Pangean paleoequator, created a rain shadow over western Pangea (Rowley et al., 1985). However, climate model simulations of the Carboniferous show the opposite effect; high CPMs focus tropical precipitation on the equator by blocking the seasonal migration of the Intertropical Convergence Zone (Otto-Bliesner, 1998, 2003). Alternatively, the drying trend has been attributed to the development of mega-monsoons on Pangea, resulting in equatorial aridity and marked seasonality (Parrish, 1993; Kessler et al., 2001). Ironically, mega-monsoon intensification may have been brought on by erosion of the CPMs (Tabor and Montañez, 2004). According to this idea, the lowering of the mountain range would have allowed the Intertropical Convergence Zone (ITCZ) to seasonally migrate away from the equator, producing seasonally-dry climates.

The Permo-Carboniferous also witnessed the deglaciation of the Gondwanan ice sheet. The Late Paleozoic glaciation began around 330 Ma and consisted of two major phases, the final of which ended rapidly in the early Permian (mid-Sakmarian) (Isbell et al., 2003.) and probably coincided with increases in atmospheric pCO_2 (Royer et al., 2006; Montañez et al., in review). Geological and oxygen isotopic evidence indicates that Late Paleozoic ice volume was as great as or greater than the Pleistocene glacial maxima (Crowley et al., 1991; Joachimski et al., 2006). The association between icehouse intervals and tropical (ever-wet, ever-warm) conditions has long been recognized. To explain this association, Ziegler et al. (1987) proposed that high pressure systems created by glaciated poles constrained the ITCZ to the equator. Cecil et al. (2003) suggested a similar mechanism, driven by orbitally-controlled glacial-interglacial cycles, to account

for Carboniferous cyclothems. However, Carboniferous climate model simulations indicate that polar ice has only a small effect on low-latitude precipitation (Otto-Bliesner, 2003).

In this contribution, we use an Earth system model, GENESIS version 2.3, to investigate the controls on Pangean tropical precipitation. Through a series of sensitivity experiments, we quantify the influence of the CPMs, Gondwanan continental ice mass, and pCO_2 on tropical precipitation. Our model results indicate that the uplift and/or erosion of the CPMs have little influence on tropical precipitation. In contrast, the deglaciation of Gondwana and increase in atmospheric CO_2 could have led to substantial decreases in tropical precipitation, though for very different reasons. The mechanism for equatorial drying in each case is investigated.

2. Tropical precipitation

In contrast to extratropical regions, tropical precipitation is largely controlled by the large-scale Hadley circulation. In the modern climate, the highest precipitation rates are associated with the upwelling branch of the Hadley cell, a region of low pressure and low-level convergence (i.e., the ITCZ). The location of the ITCZ is largely determined by surface heating rates through solar insolation, a fact that is born out by the seasonal migration of the ITCZ. This surface heating is also responsible for spawning the convective updrafts that induce high rates of precipitation. On longer timescales, however, the mean location of the ITCZ is sensitive to interhemispheric temperature contrasts, and tends to shift towards the warmer hemisphere (Broccoli et al., 2006).

The Hadley overturning is driven by diabatic heating in the tropics and cooling in the subtropics. Subtropical cooling occurs through infrared radiative cooling to space and by

energy transports to the extratropics through transient eddies (e.g., Pierrehumbert, 1995; Trenberth, 2003). The intensity of the Hadley overturning is sensitive to the tropical heating gradient; enhanced tropical heating or subtropical cooling increases the Hadley overturning (e.g., Hou and Lindzen, 1992; Kim and Lee, 2001).

In this context, long-term drying of tropical Pangea might be expected to result from either displacement of the Hadley cells or a decrease in overturning intensity. However, either of these large-scale circulation changes requires an increase in tropical heating gradients. Alternatively, the drying may be unrelated to the large-scale circulation.

3. Methods

The Late Paleozoic experiments presented here were completed using GENESIS, an earth system model that has been used extensively for paleoclimate studies. The GENESIS version 2.3 consists of an AGCM coupled to multi-layer models of vegetation, soil or land ice, and snow (Pollard and Thompson, 1995; Thompson and Pollard, 1997). Sea-surface temperatures and sea ice are computed using a 50-m slab oceanic layer with diffusive heat flux, and a dynamic sea-ice model (Flato and Hibler, 1992). The AGCM grid is independent of the surface grid: the AGCM resolution used here is spectral T31 (~3.75°) with 18 vertical levels; the surface model grid is 2x2°. The AGCM timestep is 30 minutes. A land-surface transfer model accounts for the physical effects of vegetation (Pollard and Thompson, 1995). Up to two vegetation layers (trees and grass) can be specified at each grid point, and the radiative and turbulent fluxes through these layers to the soil or snow surface are calculated. A six-layer soil model extends from the surface to 4.25 m depth, with layers thickening with depth. Physical processes in the vertical soil column include heat diffusion, liquid water transfer, surface runoff and bottom drainage,

uptake of liquid water by plant roots for transpiration, and the freezing and thawing of soil ice. A three-layer snow model is used for snow cover on soil, ice-sheet and sea-ice surfaces, including fractional cover when the snow is thin.

We conducted a series of sensitivity experiments to evaluate the influence of Gondwanan glaciation, the elevation of the Central Pangean Mountains, and atmospheric pCO_2 on low-latitude continental precipitation (Table 1). Four Late Paleozoic experiments were completed with continental ice sheets of 0.0 (NOICE), 22.8 (ICEA), 47.2 (ICEB), and 59.1 (ICEC) x 10^9 kms (Fig. 1), and mean heights of 1500m. These experiments include a Central Pangean Mountain belt with mean elevations of 1000m and an atmospheric pCO_2 of 355ppm. Two additional experiments were completed with mean belt elevations of 500 (LOMTN) and 2500m (HIMTN). A final experiment was conducted using the NOICE topography and ice-sheet extent but with atmospheric pCO_2 set to 2800ppm ($8xCO_2$). Throughout this study, the NOICE experiment will be used as the control.

All other boundary conditions were identical between experiments. The experiments include paleogeography and topography for the Sakmarian; a reduced solar luminosity (1330.3 Wm^{-2}) based on solar evolution models; Sakmarian CO_2 levels (355 ppm) (Tabor et al., 2004); pre-industrial concentrations of CH_4 (0.650 ppm) and N_2O (0.285 ppm); and a circular orbit with an average (23.5°) obliquity similar to modern. The ocean diffusive heat flux was set to a value that provides the best simulation for the modern climate. The experiments were integrated for 30 model years; the results shown here have been averaged over the final 10 years of the experiments.

4. Results

4.1 Influence of Gondwanan ice sheets

In the NOICE case, mean-annual surface temperatures range from < -20°C at the poles to > 25°C over tropical Pangea (Fig. 2). Low-latitude summer temperatures reach as high as 35 and 37°C in the subtropics of northwestern and southeastern Pangea, respectively. As demonstrated by Crowley et al. (1989) and Kutzbach and Gallimore (1989), seasonal temperature contrasts on the Pangean supercontinent are large, reaching more than 30°C at 30°S and 50°C near 60°S. The sea-ice margin reaches to almost 60°N in the Northern Hemisphere and to 70°S in the Southern Hemisphere.

The addition of Gondwanan continental ice (ICEA) causes significant cooling in the Southern Hemisphere, as much as 20° C over the ice sheet. The cooling extends into the Southern Hemisphere mid- and low latitudes; surface temperatures decrease by as much as 3° C near the equator. Even so, the influence of the Gondwanan ice sheet is largely limited to the Southern Hemisphere; annual surface temperatures in the Northern Hemisphere generally decrease by no more than 1°C (Fig. 3A). In response to cooling, the sea-ice extent expands equatorward by up to 10° in the Southern Hemisphere.

As the ice sheet grows, its influence on surface temperature increases. In comparison to the NOICE case, global mean-annual temperatures in the ICEB and ICEC experiments are 8 and 11°C cooler (Table 2), and the tropics cool by as much as 6 and 8°C over Pangea (Fig. 3B-C). Substantial cooling occurs throughout the Northern Hemisphere (Fig. 3B-C) and annual sea-ice margins expand to 50° and 55° in both hemispheres. In all three ice-sheet cases, reduced surface temperatures primarily result from an increase in surface albedo (Table 2) due to the specification of continental ice and an increase in

snow and sea-ice cover, and a reduction in the natural greenhouse effect due to a decrease in tropospheric water vapor (Table 2).

Precipitation rates and distribution on low-latitude Pangea are linked to the location and strength of the ITCZ. In the NOICE case, seasonal precipitation rates are highest in the summer hemisphere due to the seasonal migration of the ITCZ (Fig. 4), and result predominantly from atmospheric convection. In the mean annual, the tropical precipitation distribution is asymmetric with the Southern Hemisphere receiving more (Fig. 5A). This asymmetry can also be seen in the large-scale zonal circulation (Fig. 6A); the mean-annual Hadley cells are displaced southward, meeting in the low-latitudes of the Southern Hemisphere.

Tropical precipitation rates and distribution on Pangea are sensitive to the extent of the Gondwanan ice sheet. The addition of Gondwanan continental ice enhances tropical precipitation, particularly in the Northern Hemisphere, reducing the hemispheric asymmetry observed in the NOICE experiment (Fig. 5). In the ICEB and ICEC cases, zonal-average seasonal precipitation maxima increase by more than 1.0 mm day^{-1} and shift northward by up to 4° (Fig. 5). Much of the increase in precipitation occurs over western equatorial Pangea (Fig. 7). The large-scale zonal circulation is also affected by the Gondwanan continental ice. In addition to shifting northward, the mass transport of the southern cell more than doubles, while that of the northern cell decreases (Fig. 6). This response of the large-scale zonal circulation can be readily understood in terms of a heat engine that converts heat energy into mechanical energy by exploiting the temperature gradient between the heat source and sink. In such an engine, the magnitude of the temperature gradient determines the work that can be performed. Likewise, by

altering the low-latitude temperature gradient through Southern Hemisphere cooling, the addition of a large ice mass over Gondwana influences the Hadley circulation. During June-July-August, when maximum heating is in the Northern Hemisphere, the low-latitude temperature gradient is increased and the adiabatic processes that drive the Hadley circulation are enhanced, increasing mass transport in the northern Hadley cell. In contrast, during December-January-February, Southern Hemisphere cooling reduces the low-latitude temperature gradient and the adiabatic processes that drive the Hadley circulation, decreasing mass transport through the southern Hadley cell (Fig. 6).

The onset and/or intensification of monsoonal circulation in the earliest Permian has figured prominently in explanations for the long-term aridification of tropical Pangea (e.g., Kessler et al., 2001). In the NOICE case, monsoonal circulation is well established in the Southern Hemisphere. During austral summer, a prominent surface pressure low forms over southeastern Pangea, resulting in a strong cyclonic circulation. In austral winter, a surface high forms and winds are anticyclonic (Fig. 8A-B). Surface flow over western equatorial Pangea reverses direction with the monsoon. During the summer monsoon, Westerlies flow across western equatorial Pangea and into the monsoonal region. These winds become Easterlies during the winter monsoon. In comparison to the Southern Hemisphere, monsoonal circulation is less well developed over the Northern Hemisphere. A surface low centered at 25°N forms during boreal summer but engenders relatively weak cyclonic flow (Fig. 8B).

The Southern Hemisphere monsoonal circulation is strongly modified by continental ice over Gondwana. In the ICEB and ICEC experiments, the continental ice sheet intensifies the winter subtropical high and its associated anticyclonic flow in the Southern

Hemisphere. In contrast, as the continental ice area expands, the summer subtropical low weakens in the ICEA experiment, and is replaced with a surface high in the ICEB experiment (Fig. 8). This reduction in the Southern Hemisphere summer monsoon alters surface wind patterns over low-latitude Pangea; the well-developed Westerlies in the NOICE experiment are replaced by weak Easterlies (Fig. 8).

4.2 Effect of Central Pangean Mountains

In a series of sensitivity experiments using GENESIS v.1.02, Otto-Bliesner (1998, 2003) demonstrated that the Central Pangean Mountains played an important role in promoting conditions for tropical coal formation by impeding the northward migration of the ITCZ in July. Our sensitivity experiments show a similar influence of tropical mountains on tropical precipitation. In comparison to those of NOICE (intermediate CPM) and LOMTN, mean-annual continental precipitation rates in HIMNT are higher between 6°S and the equator, and lower between 10 to 20°S and 0 to 20°N (Figs. 9 and 10). These differences are consistent with high-elevation CPMs acting as an impediment to the ITCZ. Because the CPMs strike southwest-northeast, they affect the ITCZ migration during both boreal and austral summers. In June-July-August (December-January-February), high CPMs block the northward (southward) migration of the ITCZ in western (eastern) Pangea, reducing precipitation in this region. Reducing the elevation of the CPMs removes the obstacle to ITCZ migration. In the LOMTN case, continental precipitation is relatively high between 10 and 20°S, and between 5 and 20°N (Figs. 9 and 10).

Although the presence and height of the CPMs influence tropical precipitation on Pangea, the sensitivity to the CPMs is relatively small relative to atmospheric CO_2 and

the Gondwanan ice sheet. Moreover, changes in CPM elevation have only a local effect on surface temperature (Table 2). Elevated CPMs lead to an expansion of the Northern Hemisphere summer monsoonal region and a contraction of the Southern Hemisphere winter monsoonal region; however surface wind patterns show little change over low-latitude Pangea (Fig. 11).

4.3 Influence of atmospheric CO_2

On the basis of stable isotopic composition of soil-formed minerals, fossil plant matter, and shallow water brachiopods, atmospheric pCO_2 has been estimated to have increased from present atmospheric levels (PAL) in the Asselian and early Sakmarian to nearly 8x PAL by the late Sakmarian (Montañez et al., in review). To estimate the influence of the Late Paleozoic pCO_2 rise, we compare climate simulations with 1x and 8x PAL CO_2. In response to elevated pCO_2, global average surface temperatures rise by 9.6°C (Table 2). In contrast to the perennial sea-ice in the NOICE experiment, sea ice is limited to winter in the Southern Hemisphere high-latitudes. Mean-annual surface temperatures increase by 12-15°C on low-latitude Pangea, about 7°C more than low-latitude ocean temperatures (Fig. 12). The enhanced continental warming is most likely the result of a feedback with soil moisture; a rise in surface air-temperature increases evaporation, decreasing soil moisture (Fig. 13), and promoting sensible heating (i.e., surface air temperature increase) at the expense of latent heating.

Simulated tropical precipitation rates also show a large sensitivity to the pCO_2 increase. In contrast to marine precipitation rates which increase slightly, continental precipitation rates decline by as much as 40% at low latitudes (Figs. 9 and 14). The reduction in continental precipitation, like surface temperature, is directly linked to the

decrease in soil moisture. Soil moisture serves as a source of condensate and as a source of the latent heat that fuels convective updrafts. As a result, the decline in soil moisture reduces the source and the dynamical conditions that promote convective precipitation. It is interesting to note that the large reductions in tropical precipitation with higher pCO_2 are not caused by changes in the large-scale zonal circulation. The Hadley circulation in the $8xCO_2$ case is similar to that of the NOICE case (compare Figs. 6A and 15).

CO_2 has a small, but potentially important, effect on monsoonal circulation (Fig. 16). The increase in CO_2 enhances the Northern Hemisphere summer monsoon over western Pangea. This subtle intensification induces westerly flow over western equatorial Pangea (Fig. 16B).

5. Discussion

Our results suggest two possible explanations for long-term drying in equatorial Pangea. Both Southern Hemisphere deglaciation and increased atmospheric CO_2 lead to tropical drying consistent with paleofloral changes (Cleal and Thomas, 2005; Ziegler at al., 2002; Raymond and Metz, 2004), the distribution of eolian and evaporite deposits (Cecil, 1990; Rankey, 1997; Kessler et al, 2001), and $\delta^{18}O$ and stratigraphic trends in paleosols (Tabor & Montañez, 2002, 2004). However, the mechanism responsible in each case is different. The retreat of the Gondwanan ice sheet weakens the southern Hadley cell and causes it to shift southward. This reorganization of large-scale atmospheric circulation occurs as a result of the reduced temperature gradient that accompanies Southern Hemisphere warming as the ice sheet retreats. In the case of atmospheric CO_2, an increase in tropical surface temperature leads to high evaporation rates and a reduction of soil moisture, thus removing the source for convective precipitation.

Regional tectonism has previously been identified as a cause of long-term aridification in western Pangea. Our model results indicate that the CPMs can influence regional precipitation by altering the seasonal location of the ITCZ. In the zonal average, high CPMs block the northward migration of the ITCZ, reducing tropical precipitation rates in the Northern Hemisphere (Fig. 9). However, this reduction in precipitation mainly occurs over eastern tropical Pangea (Fig. 10A), little change occurs in western Pangea. We note that the regional precipitation anomalies are dependant on the orientation of the CPMs; if the CPMs had trended northwest-southeast, it is likely that their uplift would cause drying over western Pangea. But, more to the point, the CPMs have a small influence on precipitation relative to CO_2 and continental ice sheets and almost no influence on surface temperature and wind patterns. In sum, regional tectonic change was likely only a secondary control on tropical precipitation and climate.

In addition to causing low-latitude drying, both deglaciation and elevated CO_2 increase low-latitude surface temperatures over Pangea. Tabor and Montanez (2005) report a paleotemperature increase of up to 13°C over western Pangea from 22±3 to 35±3°C. Mean-annual temperatures over western Pangea are approximately 28-30°C in the NOICE experiment. Assuming that CO_2 levels were not significantly lower than 355 ppm and that other greenhouse gases were not significantly lower than modern, cooling due to the influence of continental ice on Gondwana may be required to explain the low paleotemperatures of 22°C. We note that in the ICEB experiment, mean-annual temperatures over western Pangea are 22-24°C. Likewise, the highest estimated paleotemperatures may require increases in CO_2 or other greenhouse gases. In the $8xCO_2$ experiment, mean-annual temperatures over western Pangea range are 40-42°C.

Both ice sheet retreat and increased atmospheric CO_2 induce Westerlies over western equatorial Pangea, as observed from geologic data (Soreghan, 2002). During glacial periods with extensive continental ice, low-latitude flow is predominantly westward. The contraction of continental ice allows a summer monsoon to develop over the Southern Hemisphere, inducing eastward flow over western equatorial Pangea during December-January-February (Fig. 8). In contrast, an increase in CO_2 intensifies the Northern Hemisphere summer monsoon over western Pangea, causing eastward flow over western equatorial Pangea during June-July-August (Fig. 11).

The magnitude of tropical climate change due to deglaciation is dependent on the ice sheet extent. According to the model results, reductions in precipitation are small if the ice sheets were relatively small and confined to high-latitude regions (e.g., annual decrease of 0.2 mm day^{-1} at 10°N in the ICEA case). However, the melting of larger ice sheets could lead to substantial decreases (e.g., annual decrease of 2.6 mm day^{-1} at 10°N in the ICEB case). The extent of the Permo-Carboniferous ice sheets is uncertain. Various methods have been used to determine their size. Cyclothems (Soreghan and Giles, 1999) and oxygen isotopes (Joachimski, 2006) suggest sea-level changes of 100m or greater, implying ice sheet volumes that were at least as large as those of the Pleistocene glaciations. Parrish et al. (1986) found evidence of glacial deposits reaching as far as 30°S, again indicating continental ice volumes comparable to or greater than those of the Pleistocene glaciations (Crowley et al., 1991). Moreover, simulations of Gondwanan glaciation predict large ice sheets extending to 45°S (Hyde et al., 1999). In contrast, weathering profiles and soft-sediment stratigraphy from Antarctica indicate that areas previously viewed as a glacial epicenter may have been ice-free or located along ice

margins, suggesting that Permo-Carboniferous ice coverage was less extensive than previously thought (Isbell et al., 2003). Until additional data is available to put tighter constraints on the extent of Permo-Carboniferous glaciation, it is not possible to quantify the exact influence of the Gondwanan ice sheets on low-latitude climate. Based on our model results, if the continental ice on Gondwana had approached our ICEB reconstruction, its retreat could have caused the decrease in tropical precipitation seen in the geologic record. However, we emphasize that the ICEB and ICEC reconstructions were developed for the purpose of these sensitivity studies and are highly idealized.

Most likely, a combination of effects involving deglaciation and atmospheric CO_2 rise were responsible for the Permo-Carboniferous drying trend over low-latitude Pangea. Our model results and proxy records of climate and CO_2 support this view. In a recent summary of Phanerozoic CO_2 levels, Royer (2006) reports an anti-correlation between Permo-Carboniferous glaciation and pCO_2 (i.e., low pCO_2 during Gondwanan glaciation). Moreover, as discussed above, to simulate low-latitude paleotemperatures requires a combination of pCO_2 increase and deglaciation.

6. Conclusions

This study uses the GENESIS atmospheric general circulation model to examine the sensitivity of Permian climate to continental ice extent, atmospheric CO_2 concentration, and tropical mountain elevation. We have identified two mechanisms capable of causing long-term aridification of equatorial Pangea: retreat of continental ice on Gondwana and increasing atmospheric CO_2. In both cases, drying is accompanied by warming and a reversal of low-latitude wind patterns consistent with the geological record. The uplift/erosion of low-latitude mountain ranges proves to be a secondary factor in altering

tropical climate. On the basis of geologic proxy records of CO_2 and climate and comparisons of model-predicted and proxy paleotemperatures, a combination of deglaciation and increased atmospheric CO_2 concentrations was likely responsible for the Permo-Carboniferous tropical climate changes observed over low-latitude Pangea.

Acknowledgements

We thank I. Montañez and L. Soreghan for inviting us to submit this manuscript. We gratefully acknowledge constructive comments about this work by S. Lee. This project was supported by grant (0544760) from the National Science Foundation's Sedimentary Geology and Paleontology Program to C. Poulsen.

7. References

Broccoli, A.J., Dahl, K.A., Stouffer, R.J., 2006. Response of the ITCZ to Northern Hemisphere cooling. Geophys. Res. Lett., 33, L01702.

Cecil, C.B., 1990. Paleoclimate controls on stratigraphic repetition of chemical and silicilastic rocks. Geology, 18, 533-536.

Cecil, C.B., West, R.R., Stamm, R., Wardlaw, B., Edgar, N.T., 2003. Climate controls on the stratigraphy of a Middle Pennsylvanian cyclothem in North America, Climate Controls on Stratigraphy. SEPM Special Publication 77, 151-180.

Cleal, C.J., and Thomas, B.A., 2005. Palaeozoic tropical rainforests and their effect on global climates: is the past the key to the present?. Geobiology, 3, 13-31.

Crowley, T.J., Baum, S.K., and Hyde, W.T., 1991. Climate model comparison of Gondwanan and Laurentide glaciations. J. of Geophys. Res., 96, 9217-9226.

Crowley, T.J., Hyde, W.T., and Short, D.A. 1989. Seasonal cycle variations on the supercontinent of Pangea. Geology, 17 (5), 457-460.

Flato, G.M. and Hibler III, W.D., 1992. Modeling pack ice as cavitating fluid. J. Phys. Oceanogr. , 22, 626-651.

Hou, A.Y., and Lindzen, R.S., 1992. The influence of concentrated heating on the Hadley circulation. J. Atmos. Sci., 49, 1233-1241.

Hyde, W.T., Crowley, T.J., Tarasov, L., Peltier, W.R., 1999. The Pangean ice age: studies with a coupled climate-ice sheet model. Clim. Dyn., 15 (9), 619-629.

Isbell, J.L., Miller, M.F., Wolfe, K.L., Lenaker, P.A., 2003. Timing of late Paleozoic glaciation in Gondwana: Was glaciation responsible for the development of northern hemisphere cyclothems? In: Chan, M.A., Archer, A.W. (eds.), Extreme Depositional Environments: Mega end Members in Geologic Time. Geologic Society of America Special Paper 340, Boulder, pp. 5-24.

Isbell, J.L., Lenaker, P.A., Askin, R.A., Miller, M.F., Babcock, L.E., 2003. Reevaluation of the timing and extent of late Paleozoic glaciation in Gondwana: Role of Transantarctic Mountains. Geology, 31(11), 977-980.

Joachimski, M.M., von Bitter, P.H., Buggisch, W., 2006. Constraints on Pennsylvanian glacioeustatic sea-level changes using oxygen isotopes of conodont apatite. Geology, 34 (4), 277-280.

Kessler, J.L.P., Soreghan, G.S., Wacker, H.J., 2001. Equatorial Aridity in Western Pangea: Lower Permian Loessite and Dolomitic Paleosols in Northeastern New Mexico, U.S.A.. J. Sediment. Res., 71 (5), 817-832.

Kim, H.-K., and Lee, S., 2001. Hadley cell dynamics in a primitive equation model. Part II: Nonaxisymmetric flow,.J. Atmos. Sci., 58, 2859-2871.

Kutzbach, J.E. and Gallimore, R.G. 1989. Pangaean climates: Megamonsoons of the megacontinent. J. of Geophys. Res., 94 (D3), 3341-3357.

Loope, D.B., Stiener, M.B., Rowe, C.M., Lancaster, N., 2004. Tropical westerlies over Pangean sand seas. Sedimentology 51, 315-322.

Montañez, I.P., Tabor, N.J., Niemeier, D., DiMichele, T.D., Frank, C.R., Fielding, J.L., Isbell, J.L., Birgenheier, L.P., Rygel, M.C., CO_2-forced climate instability and linkages to tropical vegetation during Late Paleozoic deglaciation. in press.

Otto-Bliesner, B.L., 1998, Effects of tropical mountain elevations on the climate of the Late Carboniferous: Climate model simulations. In: Crowley, T.J. and Burke, K.C.,

(eds.), Tectonic Boundary Conditions for Climate Reconstructions. Oxford Monographs on Geology and Geophysics, 39, 100-115.

Otto-Bliesner, B., 2003. The Role of Mountains, Polar Ice, and Vegitation in Determining the Tropical Climate during the Middle Pennsylvanian: Climate Model Simulations, Climate Controls on Stratigraphy. SEPM Special Publication 77, 227-237.

Parrish, J.T., 1993. Climate of the supercontinent Pangea. J. Geology, 101, 215-233.

Parrish, J.M., Parrish, J.T., Ziegler, 1986. Permian-Triassic paleogeography and paleoclimatology and implications for Therapsid distribution. In: Hotton, N II, McLean, P.D., Roth, J.J., Roth, E.C. (eds.), The ecology and biology of mammal-like reptiles. Smithsonian Instruction Press, 109-131.

Pierrehumbert, R.T., 1995. Thermostats, radiator fins, and the local runaway greenhouse. J. Atmos. Sci., 52, 1784-1806.

Pollard, D. and Thompson, S.L., 1995. Use of a land-surface-transfer scheme (LSX) in a global climate model (GENESIS): The response to doubling stomatal resistance. Global and Planetary Change, 10, 129-161.

Raymond, A., Metz, C., 2004. Ice and Its Consequences: Glaciation in the Late Ordovician, Late Devonian, Pennsylvanian-Permian, and Cenozoic Compared. The J. Geology, 112, 655-670.

Rankey, E., 1997. Relations between relative changes in sea level and climate shifts: Pennsylvanian-Permian mixed carbonate-siliclastic strata, western United States. GSA Bulletin, 109 (9), 1089-1100.

Rowley, D.B, Raymond, A., Parrish, J.T., Lottes, A.L., Scotese, C.R., Ziegler, A.M., 1985. Carboniferous Paleogeographic, phytogeographic, and paleoclimatic reconstructions. Int. J. Coal. Geol., 5, 7-24.

Royer, D.L., 2006. CO_2-forced climate thresholds during the phaerozoic. Geochim. Cosmochim. Acta, in press.

Scotese, C.R., 1999. PALEOMAP Animations 'Paleogeography'. PALEOMAP Project. Department of Geology, University of Texas, Arlington, TX.

Soreghan, G.S., Giles, K.A., 1999. Amplitudes of Late Pennsylvanian glacioeustasy. Geology, 27 (3), 255-258.

Soreghan, M.J., Soreghan, G.S., Hamilton, M.A., 2002. Paleowinds inferred from detrital-zircon geochronology of upper Paleozoic loessite, western equatorial Pangea. Geology 30 (8), 695-698.

Tabor, N.J., and Montañez, I.P., 2002. Shifts in late Paleozoic atmospheric circulation over western equatorial Pangea: Insights from pedogenic mineral $\delta^{18}O$ compositions. Geology 30 (12), 1127-1130.

Tabor, N.J., and Montañez, I.P., 2004. Morphology and distribution of fossil soils in the Permo-Pennsylvania Wichita and Bowie Groups, north-central Texas, USA: implications for western equatorial Pangean paleoclimate during icehouse-greenhouse transition. Sedimentology, 51, 851-884.

Tabor, N.J., and Montañez, I.P., 2005. Oxygen and hydrogen isotope compositions of Permian pedogenic phyllosilicates: Development of modern surface domain arrays and implications for paleotemperature reconstructions. Palaoegeogr., Palaeoclimatol., Palaeoecol., 223, 127-146.

Thompson, S. L., and Pollard, D., 1997. Greenland and Antarctic mass balances for present and doubled atmospheric CO_2 from the GENESIS version-2 global climate model. J. Climate, 10(5), 871-900.

Trenberth, K.E., and Stepaniak, D.P., 2003. Seamless poleward atmospheric energy transports and implications for the Hadley circulation. J. Climate, 16, 3706-3722.

Ziegler, A.M., Raymond, A.L., Gierlowski, T.C., Horrell, M.A., Rowley, D.B., and Lottes, A.L., 1987. Coal, climate and terrestrial productivity: the present and early Cretaceous compared, in Scott, A.C., ed., Coal and coal-bearing strata: recent advances. Geol. Soc. Lond. Spec. Publ., 25-49.

Ziegler, A.M., Rees, P., and Naugolnykh, S.V., 2002. The Early Permian floras of Prince Edward Island, Canada: differentiating global from local effects of climate change. Can. J. Earth Sci., 39, 223-238.

Table 1. List of Late Paleozoic climate model experiments.

Experiment	Ice Sheets	Paleogeography	Atmospheric pCO_2
CNTRL	None	1000m tropical mountains	355 ppm
ICEA	Small extent	1000m tropical mountains	355 ppm
ICEB	Intermediate extent	1000m tropical mountains	355 ppm
ICEC	Large extent	1000m tropical mountains	355 ppm
LOMTN	None	500m tropical mountains	355 ppm
HIMTN	None	2500m tropical mountains	355 ppm
$8xCO_2$	None	1000m tropical mountains	2800 ppm

Table 2. Mean-annual global averages for the Late Paleozoic climate model experiments.

Experiment	Surface albedo	Greenhouse effect	Surface temperature
CNTRL	0.302	180	13.2
ICEA	0.318	177	11.0
ICEB	0.354	168	5.2
ICEC	0.373	162	1.8
LOMTN	0.301	181	13.4
HIMTN	0.302	180	13.0
$8xCO_2$	0.274	193	22.8

Figure Captions

Figure 1. Late Paleozoic geography. An early Permian land-ocean distribution is used in all experiments. The continental ice-sheet extents are shown in white for the B) ICEA, C) ICEB, and D) ICEC experiments. The Central Pangean Mountain topography is contoured (500m interval) in A.

Figure 2. Mean-annual (A), June-July-August (B), and December-January-February (C) surface temperature (°C) for the control (NOICE) experiment.

Figure 3. Mean-annual surface temperature differences (°C). The differences represent A) ICEA – NOICE, B) ICEB – NOICE, and C) ICEC – NOICE. Note that the contour interval is not constant.

Figure 4. Mean-annual (A), June-July-August (B), and December-January-February (C) average precipitation rates (mm day^{-1}) for the control (NOICE) experiment. The seasonal migration of the precipitation maxima can be seen in B and C, and coincides with the position of the ITCZ. Note that the contour interval is not constant.

Figure 5. Zonal-average continental precipitation (mm day^{-1}). The zonal precipitation is shown for mean-annual (A), June-July-August (B), and December-January-February (C) averages. Results are for the NOICE, ICEA, ICEB, and ICEC experiments.

Figure 6. Annual-mean zonal streamfunction (10^9 kg s^{-1}). The streamfunction is shown for NOICE (A), ICEA (B), ICEB (C), and ICEC (D) experiments. Solid (dashed) lines represent (counter) clockwise overturning circulation. The expansion of continental ice in the ICEB and ICEC experiments causes the overturning intensity in the southern cell to increase by 100% or more. The contour interval is 20 x 10^9 kg s^{-1}.

Figure 7. Mean-annual (A), June-July-August (B), and December-January-February (C) average precipitation rates differences (mm day^{-1}) between the ICEC and NOICE experiments (ICEC – NOICE). The addition of a large ice sheet on Gondwana causes the ITCZ to shift northward into the Northern Hemisphere during JJA.

Figure 8. December-January-February (left) June-July-August (right) sea-level pressure (mb) and winds (m^2s^{-2}). SLP and winds are illustrated for the NOICE (A-B), ICEA (C-D), ICEB (E-F), and ICEC (G-H) experiments.

Figure 9. Zonal-average continental precipitation (mm day^{-1}). The zonal precipitation is shown for mean-annual (A), June-July-August (B), and December-January-February (C) averages. Results are from the NOICE, HIMTN, LOMNT, and 8xCO_2 experiments.

Figure 10. Mean-annual (A, D), June-July-August (B, E), and December-January-February (C, F) average precipitation rates differences (mm day^{-1}). The left column shows differences between the HIMTN and control (NOICE) cases (HIMTN – NOICE). The right column shows differences between the LOMTN and control (NOICE) cases

(LOMTN – NOICE). Note that high CPMs tend to block the seasonal migration of the ITCZ, reducing precipitation off the equator.

Figure 11. December-January-February (left) and June-July-August (right) sea-level pressure (mb) and winds (m^2s^{-2}). SLP and winds are illustrated for the LOMTN (top) and HIMTN (bottom) experiments.

Figure 12. Mean-annual surface temperature difference (°C) between the $8xCO_2$ and control experiment ($8xCO_2$ – NOICE).

Figure 13. Mean-annual soil wetness difference (%) between the $8xCO_2$ and control experiment ($8xCO_2$ – NOICE). The increase in CO_2 results in higher temperature and a large decrease in soil moisture at low latitudes.

Figure 14. Mean-annual (A), June-July-August (B), and December-January-February (C) average precipitation rates differences (mm day^{-1}) between the $8xCO_2$ and control experiment ($8xCO_2$ – NOICE). High pCO_2 causes drying over low-latitude Pangea.

Figure 15. Annual-mean zonal streamfunction (10^9 kg s^{-1}) for the $8xCO_2$ experiment. The overturning circulation in the $8xCO_2$ experiment is similar to the NOICE experiment (compare with Fig. 7). The contour interval is 20 x 10^9 kg s^{-1}.

Figure 16. December-January-February (A) and June-July-August (B) sea-level pressure (mb) and winds (m^2s^{-2}) for the $8xCO_2$ experiment.

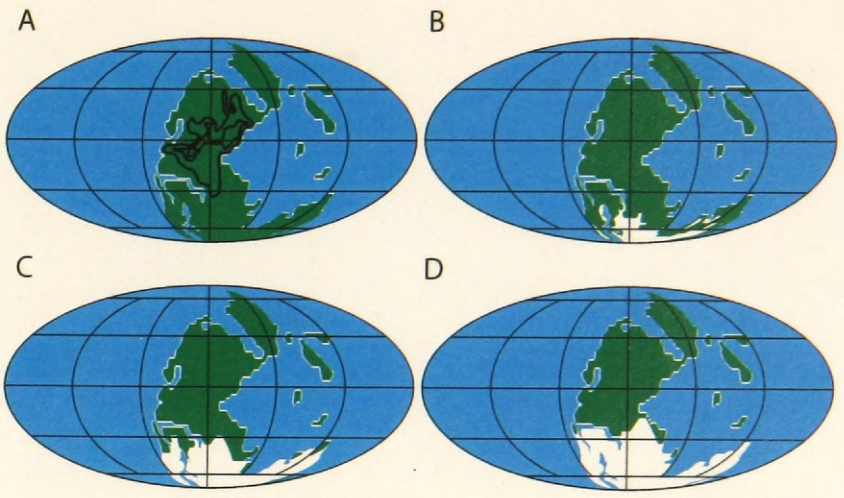

Figure 1

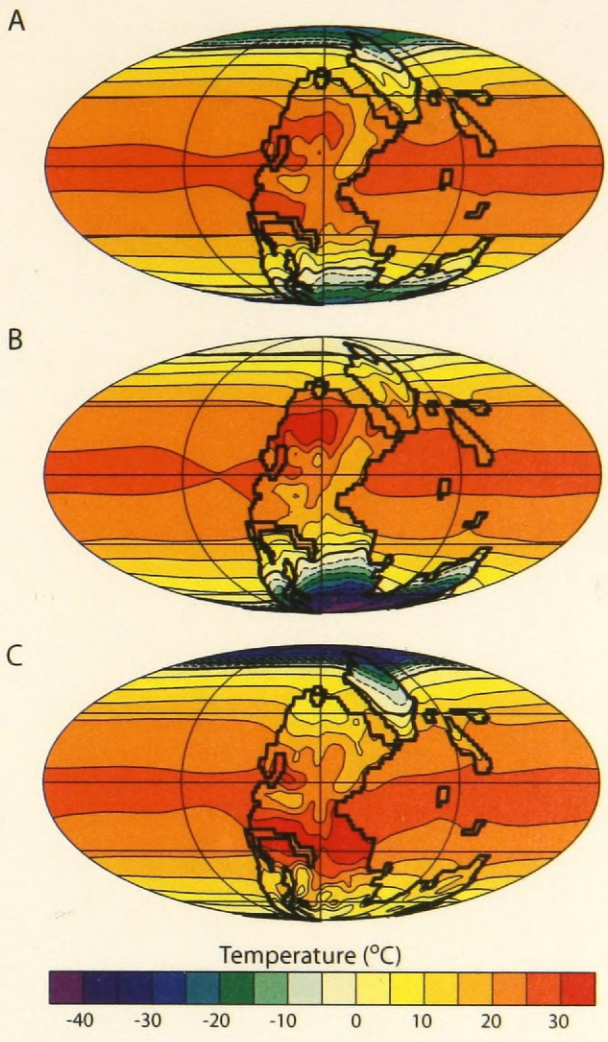

Figure 2

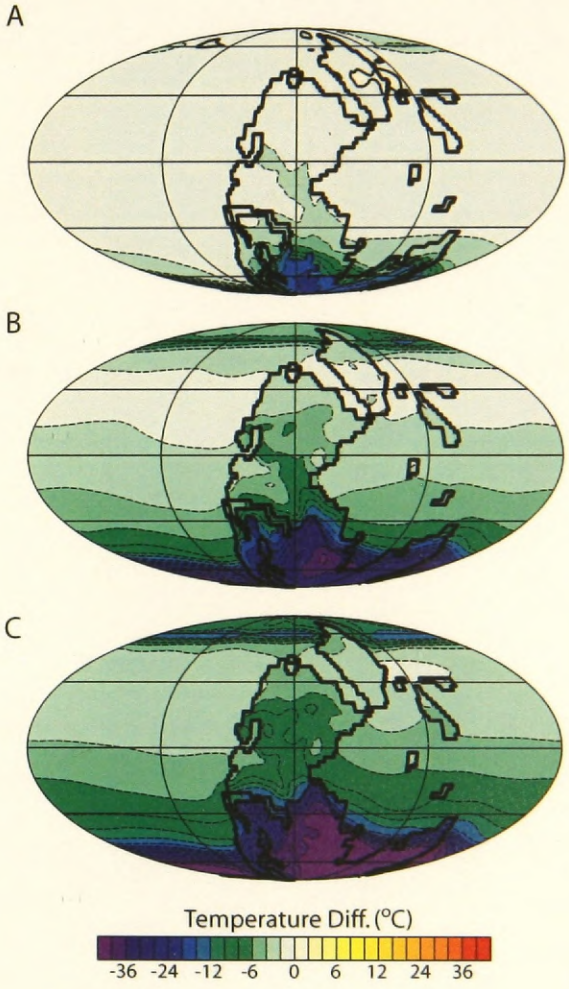

Figure 3

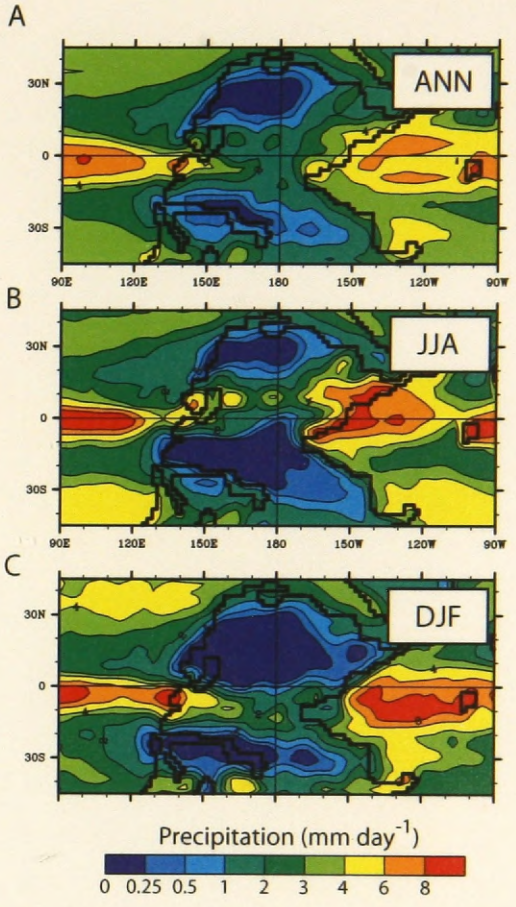
A
ANN
30N
0
30S
90E
120E
150E
180
150W
120W
90W
B
JJA
30N
0
30S
90E
120E
150E
180
150W
120W
90W
C
DJF
30N
0
30S
Precipitation (mm day-1)
0 0.25 0.5 1 2 3 4 6 8

Figure 4

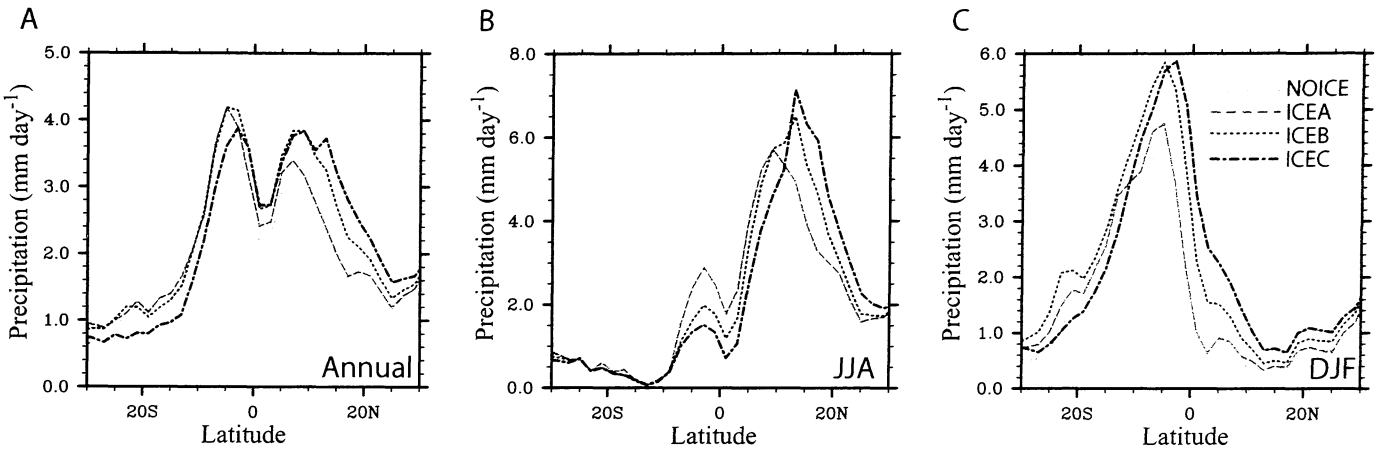
A
B
C
Precipitation (mm day-1)
Latitude
20S
0
20N
Annual
JJA
DJF
NOICE
ICEA
ICEB
ICEC

Figure 5

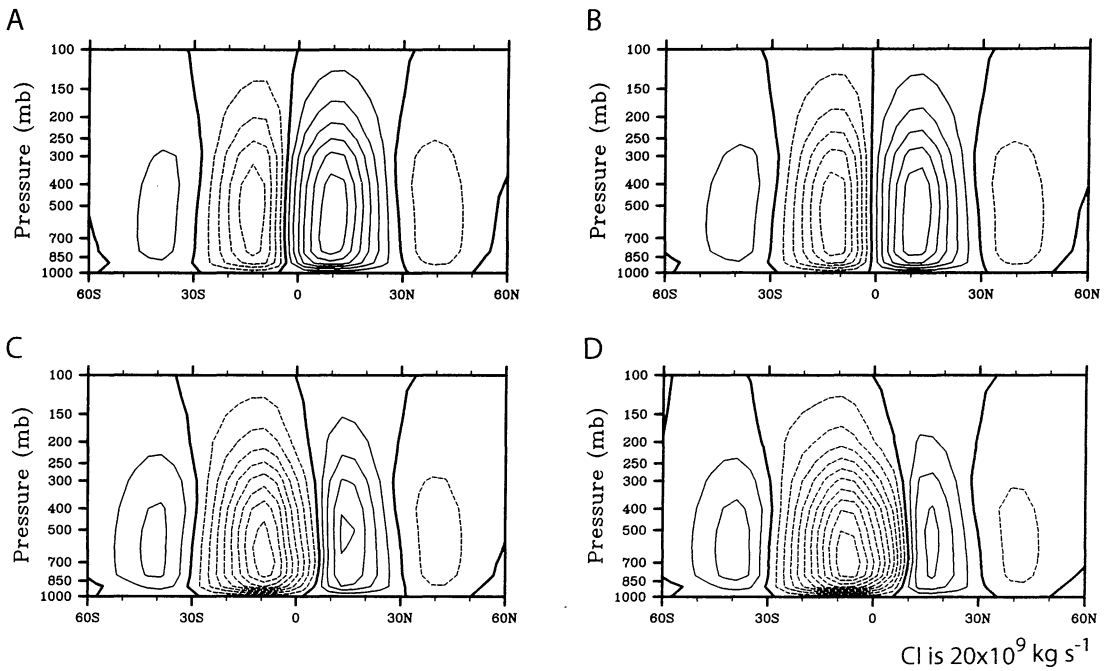
A
B
C
D
Pressure (mb)
100
150
200
250
300
400
500
700
850
1000
60S
30S
0
30N
60N
CI is 20x10^9 kg s^-1

Figure 6

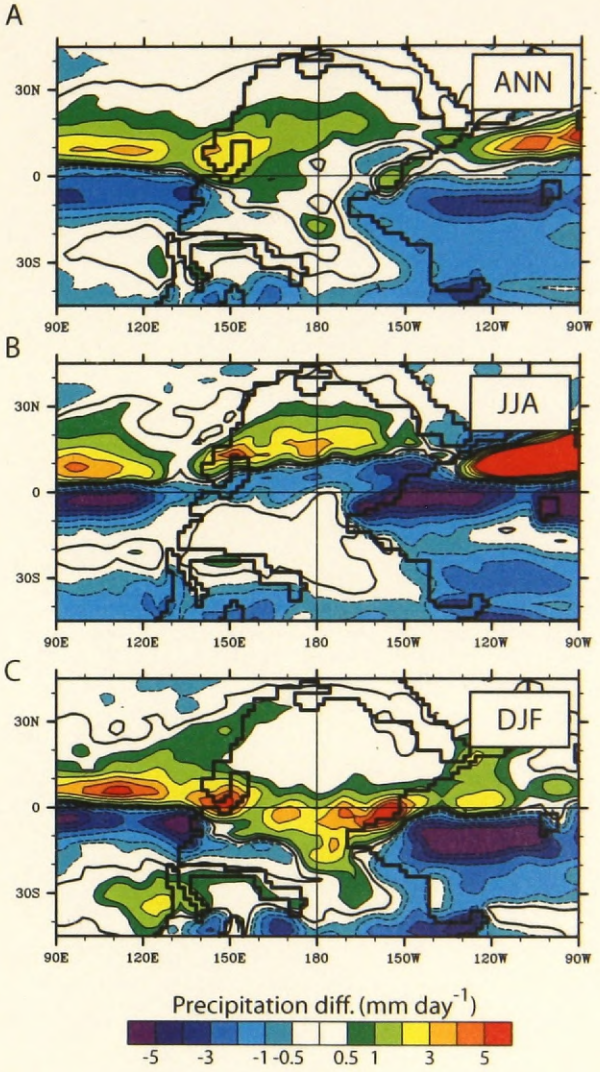
A
ANN
30N
0
30S
90E
120E
150E
180
150W
120W
90W
B
JJA
30N
0
30S
90E
120E
150E
180
150W
120W
90W
C
DJF
30N
0
30S
90E
120E
150E
180
150W
120W
90W
Precipitation diff. (mm day-1)
-5
-3
-1
-0.5
0.5
1
3
5

Figure 7

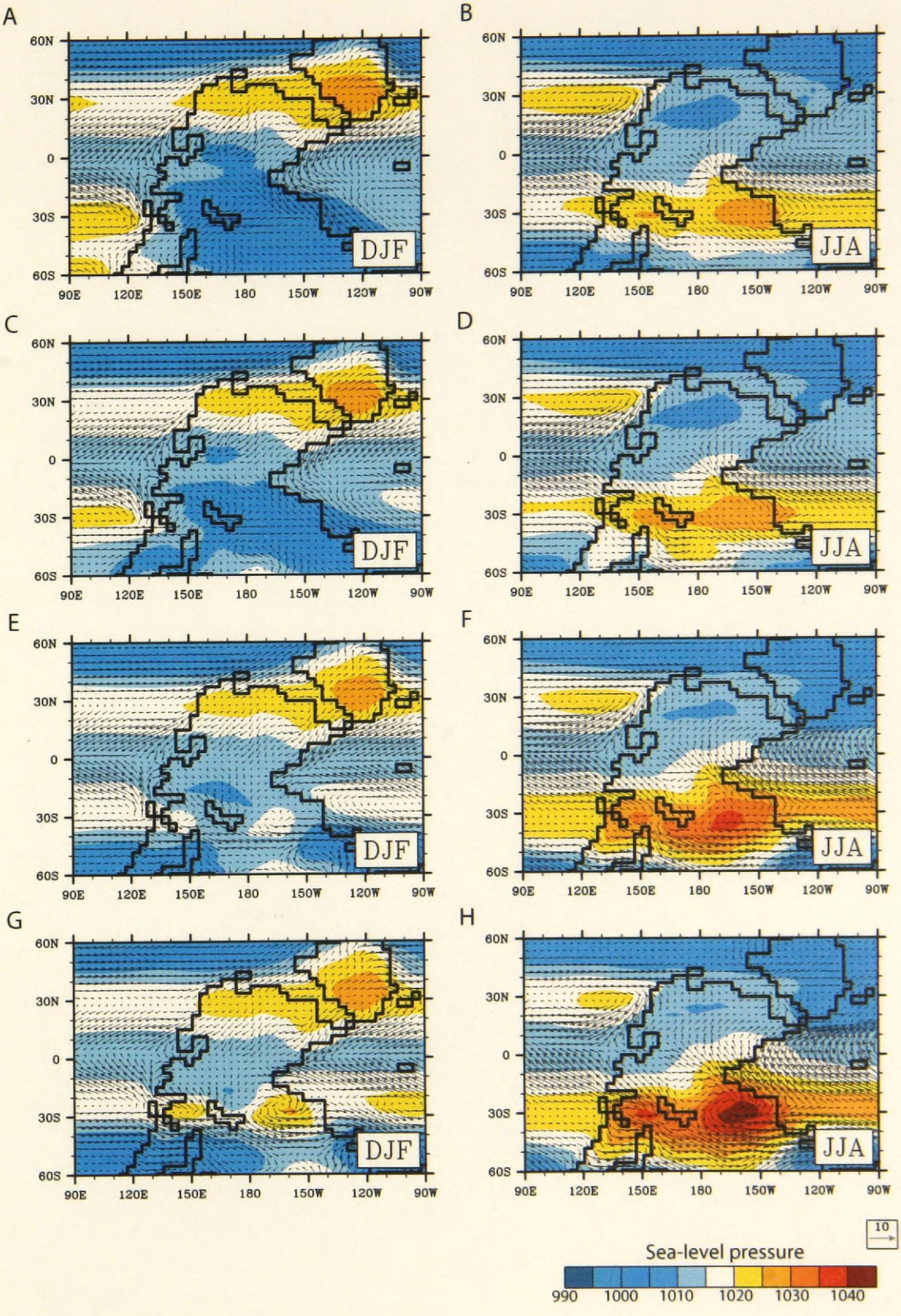
A
B
C
D
E
F
G
H
DJF
JJA
60N
30N
0
30S
60S
90E
120E
150E
180
150W
120W
90W
10
Sea-level pressure
990
1000
1010
1020
1030
1040

Figure 8

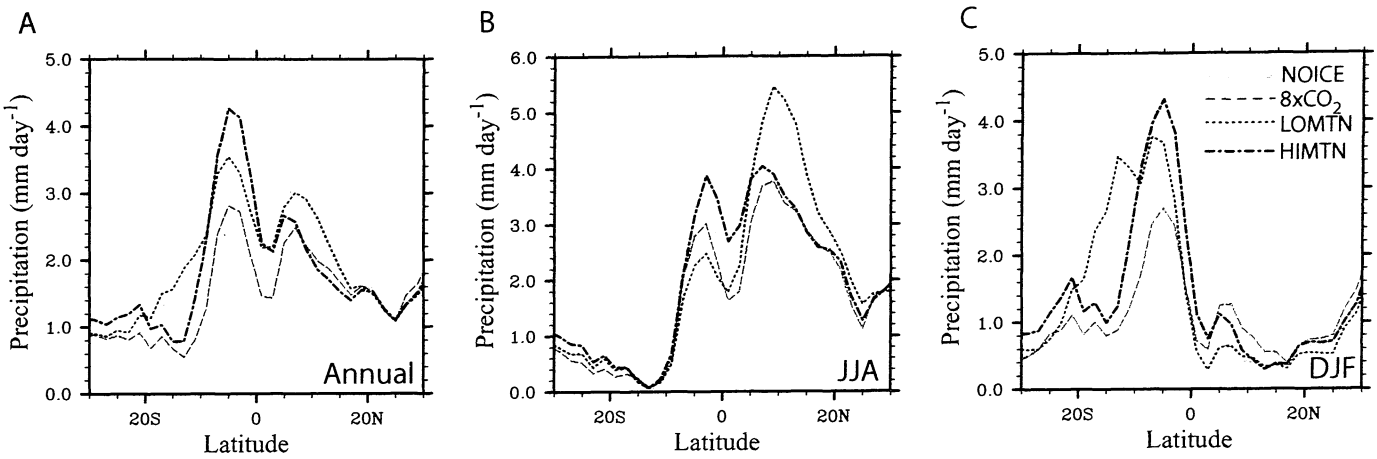
A
B
C
Precipitation (mm day-1)
Latitude
20S
0
20N
Annual
JJA
DJF
NOICE
8xCO2
LOMTN
HIMTN

Figure 9

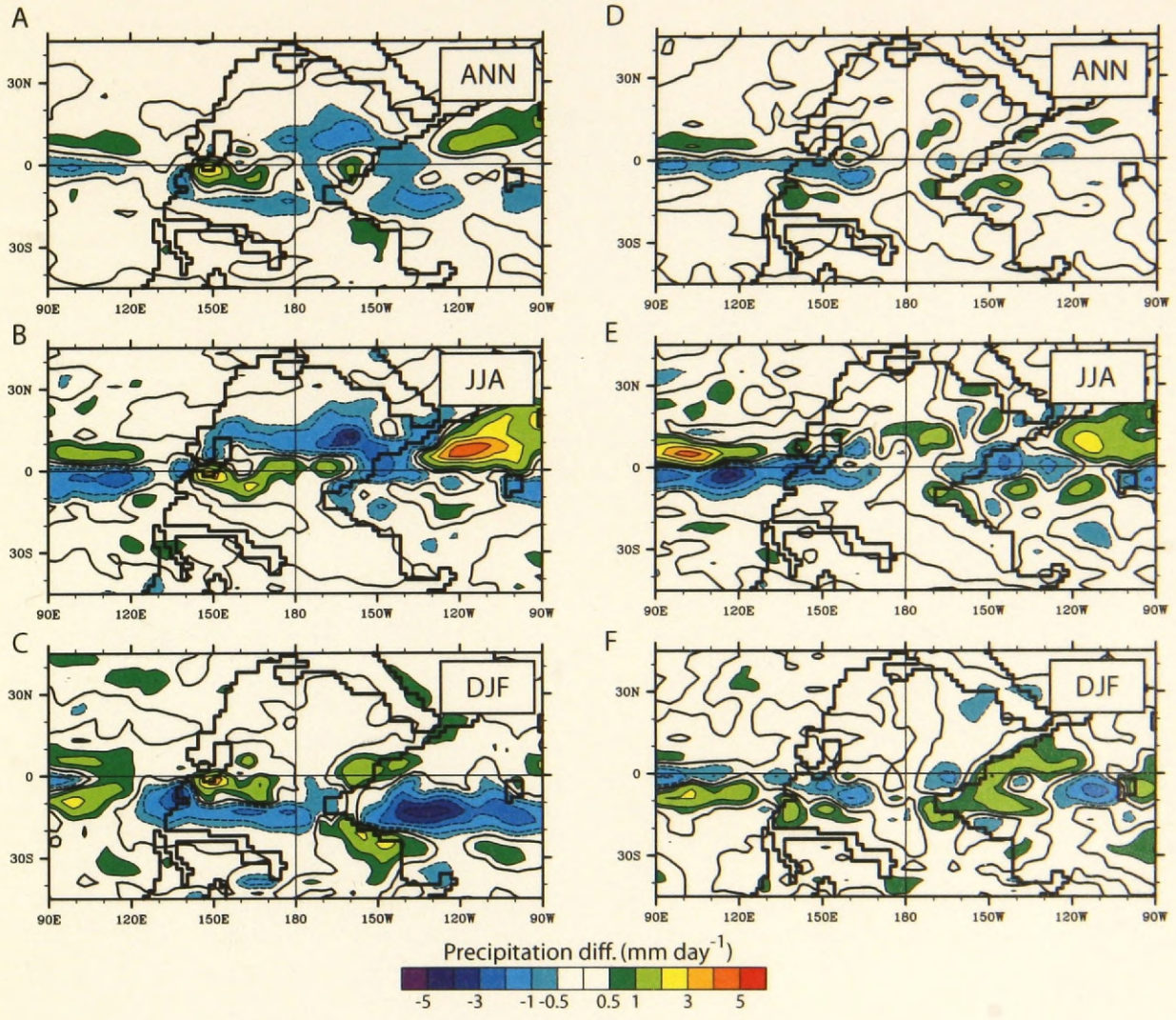
A
ANN
B
JJA
C
DJF
D
ANN
E
JJA
F
DJF
30N
0
30S
90E
120E
150E
180
150W
120W
90W
Precipitation diff. (mm day-1)
-5
-3
-1
-0.5
0.5
1
3
5

Figure 10

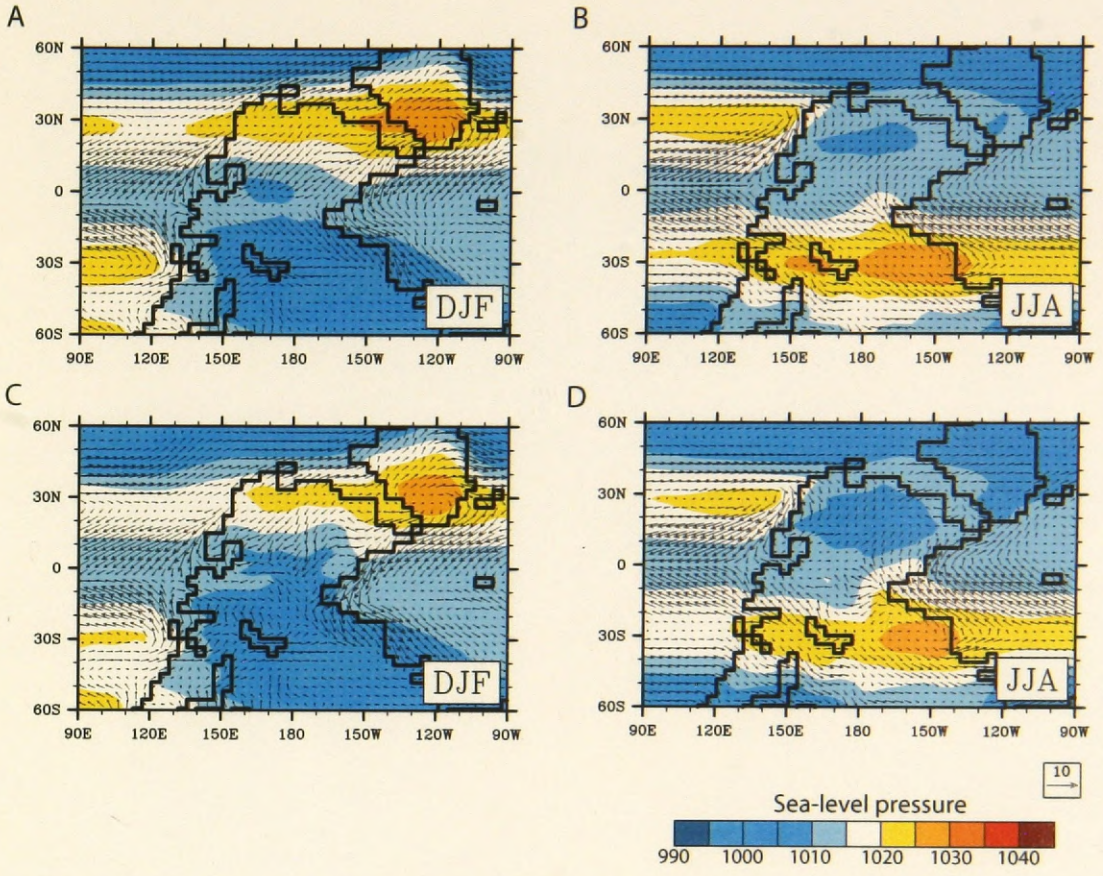
A
B
C
D
60N
30N
0
30S
60S
90E
120E
150E
180
150W
120W
90W
DJF
JJA
DJF
JJA
10
Sea-level pressure
990
1000
1010
1020
1030
1040

Figure 11

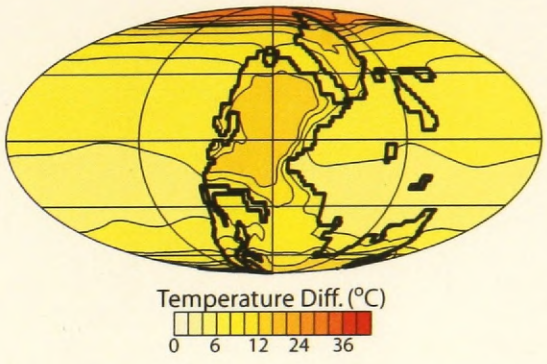

Figure 12

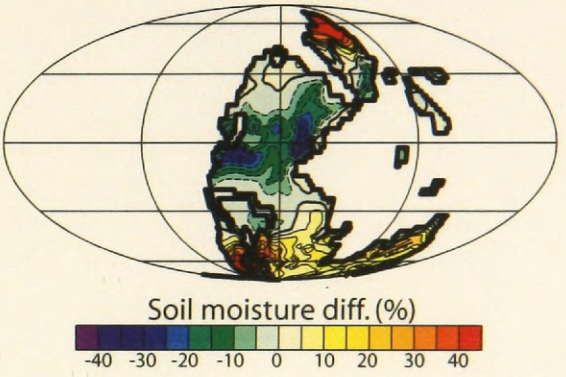

Figure 13

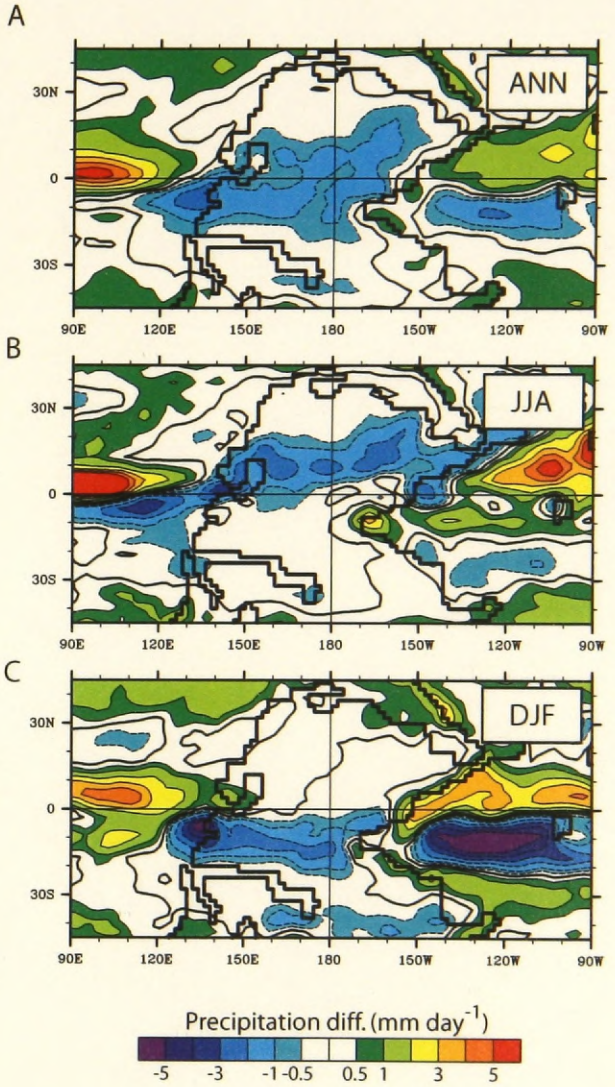
A
ANN
30N
0
30S
90E
120E
150E
180
150W
120W
90W
B
JJA
C
DJF
Precipitation diff. (mm day-1)
-5
-3
-1
-0.5
0.5
1
3
5

Figure 14

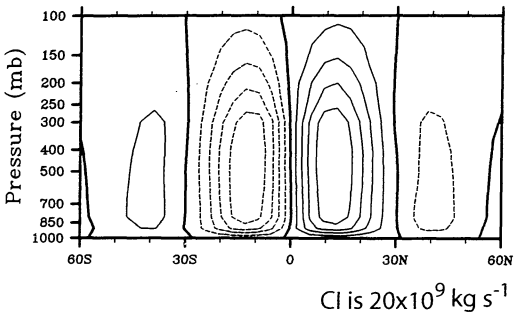
Pressure (mb)
100
150
200
250
300
400
500
700
850
1000
60S
30S
0
30N
60N
CI is 20x10^9 kg s^-1

Figure 15

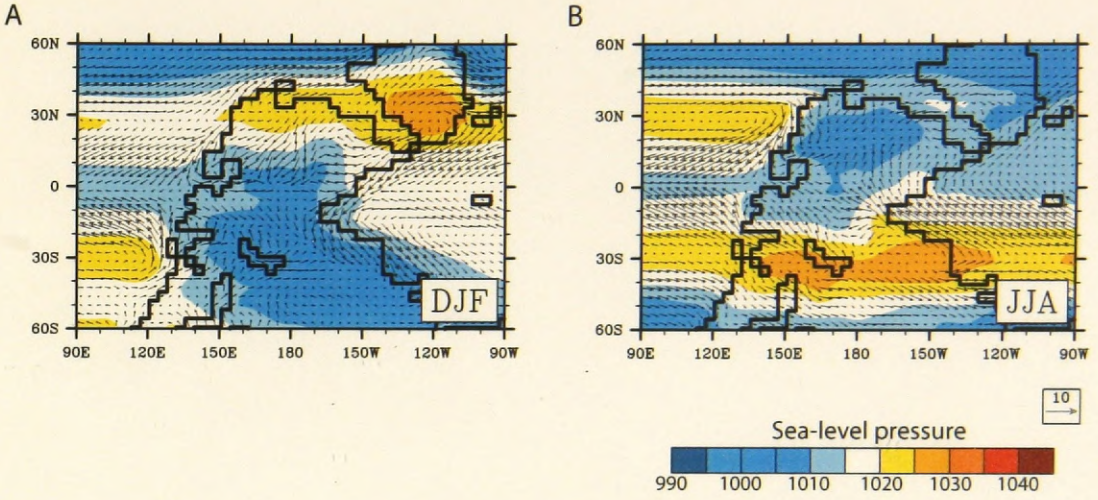
A
B
60N
30N
0
30S
60S
90E
120E
150E
180
150W
120W
90W
DJF
JJA
10
Sea-level pressure
990
1000
1010
1020
1030
1040

Figure 16